Investigation on the flexibility of chiral tricyclic derivatives†

Maria Altamura,[a] Paolo Dapporto,[b] Antonio Guidi,[a] Nicholas J. S. Harmat,[a] Loïc Jierry,[a] Elisa Libralesso,[a] Paola Paoli*[b] and Patrizia Rossi[b]

Received (in Durham, UK) 29th January 2008, Accepted 18th April 2008
First published as an Advance Article on the web 30th June 2008
DOI: 10.1039/b801569d

In the perspective of generating libraries for broad screening purposes, the inversion barrier of enantiomeric conformers of various tricyclic compounds, characterized by a seven-membered ring featuring a lactam group with two aromatics condensed at its opposite sides, has been investigated by *ab initio* calculations and NMR spectroscopy. Solid-state structure characterizations by single-crystal X-ray diffraction have been also carried out. The aim was to assess if moving from ethers to sulfides and sulfones derivatives, causes the racemization barrier to vary. Investigation was also extended to thiolactam congeners. Structural and electronic effects were investigated on the energetics of the inversion process and structure-property relationships evidenced. Results suggest that the ring inversion of the oxo derivatives is easier with respect to the corresponding S/SO_2 ones. Also amide molecules have, on the whole, smaller barriers with respect to the corresponding thioamide ones.

Introduction

The control of internal motions in molecules targeted to be high affinity protein binders is object of much consideration at the beginning of drug discovery projects. Often, once a hit has been identified, a possible strategy consists in synthesizing less flexible analogues, the structure of which is sometimes suggested by computer aided drug design. Since the need of flexibility modulation appears to be essentially target independent, we speculated that the lead finding phase could be sped up by properly managing both diversity and conformational flexibility in pools of pre-synthesized ligand candidates. As for the flexibility issue, in a first study,[1] we considered the derivatives of 3,5-*trans*-dihydroxypiperidine in which nitrogen inversion and ring flipping characterize the internal motions (Fig. 1).

We observed that nitrogen oxidation precludes inversion and unbiases ring flipping in a way that can be modulated by the ability as hydrogen bond donors of the substituents at positions 3 and 5. Later, tertiary diamides of *o*-phthalic acid were considered. Early in this second study,[2] we observed that the steric hindrance of substituents at positions 3 and 6 slows down both amide *cis–trans* isomerization and double vicinal C_{ar}–CO inversion. Subsequently,[3] we found that changes in the same direction can be attained by single and double amide thionation (Fig. 2). During this part of the work, we took into consideration the difference existing between the pharmaceutical and pharmacological time scale[4] and succeeded in accumulating and testing an isomer, in any case a racemate, separately from its conformational mixture.[5]

As for chirality, when *o*-phthalic acid is doubly condensed with two secondary amines not contributing with any stereogenic element, the corresponding pool is composed of both diastereoisomeric and enantiomeric conformers. Conversely, since the piperidine scaffold possesses two kinetically stable stereogenic centres, the related flexibility scale involves only diastereoisomeric conformers, the ensemble of the corresponding enantiomers being achievable separately by synthesis.[6] Since stereoselectivity is an important issue in protein binding, we sought more recently what constitutes the matter of this contribution: a way to modulate flexibility by contemplating only enantiomers with different racemization barriers. On the basis of the well-known drug applicability of the substrates and our previous experience in the field,[7] we turned our attention to tricyclic compounds characterized by a seven-membered ring holding together two aromatics condensed at its opposite sides. In some cases, these compounds are chiral for the distinguishability of the aromatic rings (compounds of type A) (Fig. 3).[8–10] In other cases, the same condition is not necessary (compounds of type B).[11,12]

We decided to focus on type B compounds also because the presence of a lactam bond could link to the work on phthalic

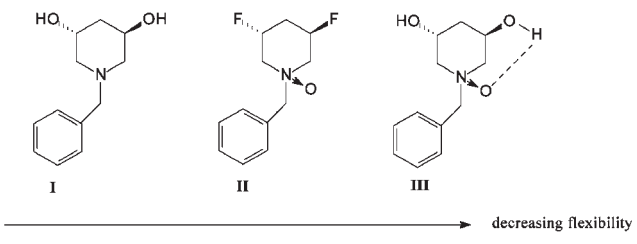

Fig. 1 Derivatives of 3,5-*trans*-dihydroxypiperidine ranked accordingly to their different flexibility.[1] For diversity, imagine substitutions at the aromatic moiety, as well as HNCOR group in the place of hydroxyl groups in molecules **I** and **III**, and MeNCOR replacing fluorine atoms in molecule **II**.

[a] *Chemistry Department, Menarini Ricerche S.p.A., Florence, Italy*
[b] *Department of Energy Engineering "Sergio Stecco", University of Florence, Italy. E-mail: paolapaoli@unifi.it*

† CCDC reference numbers 685693–685695. For crystallographic data in CIF or other electronic format see DOI: 10.1039/b801569d

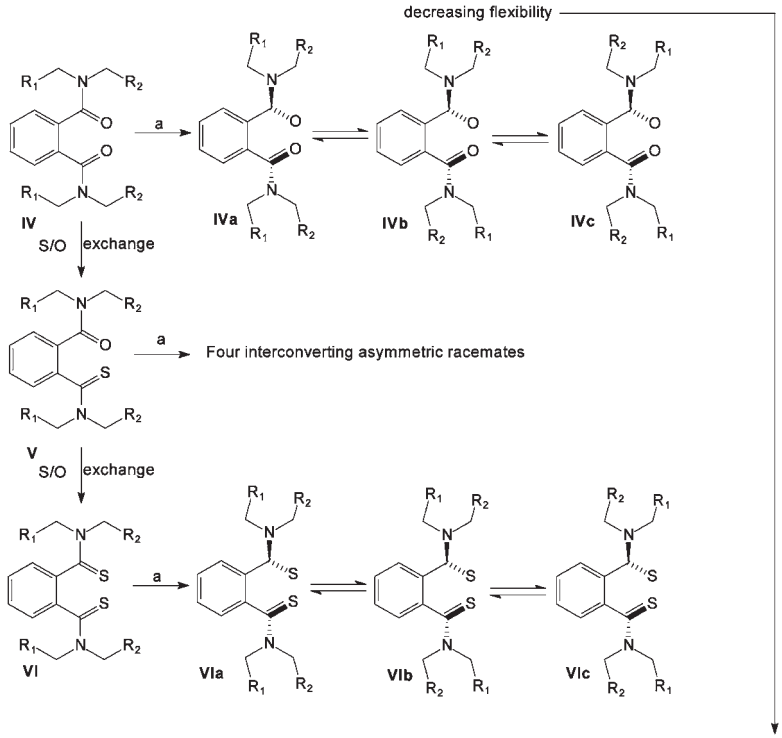

Fig. 2 Tertiary dioxo- (**IV**), oxothio- (**V**) and dithio- (**VI**) amides of *o*-phthalic acid (together with their conformational isomers), ranked accordingly to their decreasing flexibility.[3] For diversity, imagine different R_1 and R_2 substituents, as well as substituents symmetrically juxtaposed at the aromatic moiety of *o*-phthalic acid, once paid attention to the fact that especially those at positions 3 and 6 can contribute to dictate the speed of the conformational interconversion.

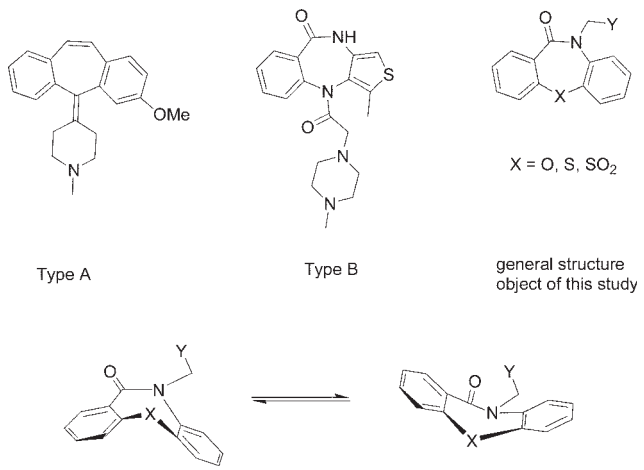

Fig. 3 Top left: examples of dissymmetrically chiral tricyclic compounds (types A and B); Top right: schematic drawing of the compounds object of this study; Bottom; isomers interconversion of type B molecules.

acid diamides. Actually, the idea was to modulate the racemization barrier by changing the nature of the group "X". To this regard, we thought that ethers, sulfides and sulfones (X = O, S, and SO_2, respectively) could be investigated earlier, standing the commercial availability of the secondary lactam precursors and the putative simplicity of the required additional synthetic chemistry. Of course, the diversity within the hypothetical pool had to be initially restricted only to the substituent "Y", placed far enough from the tricycle to avoid interference with the inversion mechanism. With this in mind, we describe here a physico-chemical study dealing experimentally with compounds **1–3** and, theoretically with compounds **4–9** (Fig. 4).

Compounds **1–3** were studied either in the solid state by single-crystal X-rays analysis, or in solution as the corresponding methyl esters (**12–14**) (Scheme 1), by NMR spectroscopy. The carboxy group was chosen as a model of "Y" appendage, in the perspective to attempt the crystallization induced dynamic resolution of the most rigid congener by enantiopure bases.[13] Similarly, the single methylene spacer was chosen so to have an isolated chirality marker suitable for dynamic NMR investigation. In parallel, theoretical calculations were performed on compounds **4–6**, to determine the inversion

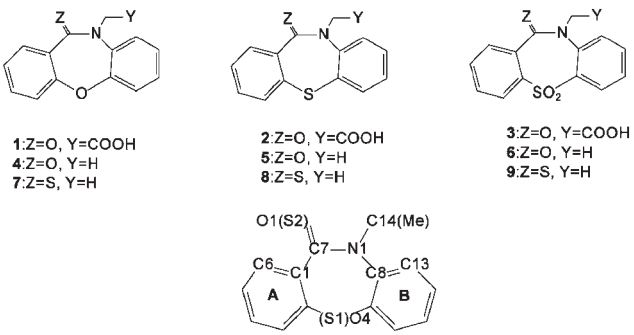

Fig. 4 Schematic drawings of the molecules characterized by single-crystal X-ray diffraction (**1–3**) and those used in the computational study (**4–9**). Below: drawing with the atom labelling conforms to the X-ray structures, when possible.

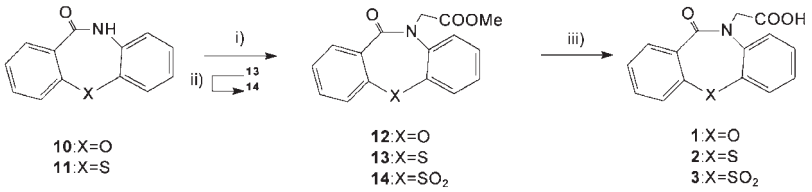

i) NaH, $BrCH_2COOMe$, DMF, 70°. X=O, 91%. X=S, 79%. ii) mCPBA, DCM, RT. 88%
iii) NaOH, refluxing CH_3OH. X=O, 68%. X=S, 78%. X=SO_2, 78%.

Scheme 1 Synthetic pathway for compounds **1–3**.

barriers in the gas phase and to understand the chemical factors dictating their values. Eventually, the theoretical study was extended to compounds **7–9** aiming ultimately at expanding the range of reduced flexibility by hopping from the lactam to the thiolactam group, in analogy with the previous work on *o*-phthalic acid diamides.

Literature background

The seven-membered ring connecting the two aromatic moieties is not planar, and in the presence of an unsaturated bond it usually shows a boat conformation, the inversion of which generates two enantiomers according to Fig. 3. Compound 5-ethyl-5,6-dihydro-11*H*-dibenzo[*b*,*e*]-6-one and the corresponding thiolactam are published examples of this phenomenon.[14] In that study, Irurre *et al.* noted that the inversion energy barrier increased with the size of the N1 substituent (R) when moving from lactam to thiolactam derivative (^{1}H DNMR data). Irurre rationalised the measured $\Delta G^{\neq}$ trend on the basis of the increasing steric effects of R, which enhance the instability of the planar transition state. Importantly, the same effect of the N1 substituent size on the inversion barrier has been also evidenced in 1,4-benzodiazepine (BZD) derivatives.[15] The DFT optimised ring-inversion transition structures of BZD derivatives obtained by Carlier have the seven-membered ring almost flat and show a loss of the amide resonance when larger R groups are present (R = *i*-Pr, R = $CHPh_2$). Analogous results were obtained from a computational study performed by Paizs and Simonyi,[16] mainly directed to elucidate the effect of the benzoannulation and of the phenyl ring on the C5 atom of the 1,4-diazepine. In all the cited reports the measured and/or calculated inversion barrier is too low, namely <21 kcal mol^{-1}, to allow the separation of the enantiomers at room temperature, thus, in all cases the compounds exist as conformational racemates.

Results and discussion

Synthesis

The synthesis of compounds **1–3** was accomplished as outlined in Scheme 1. Commercially available compounds **10** and **11** were alkylated with methyl bromoacetate in DMF at 70° to give the esters **12** and **13**. Compound **13** was then oxidized to the corresponding sulfone **14** by *m*CPBA at room temperature. The three esters **12**, **13** and **14** were eventually saponified in refluxing methanol to give compounds **1–3**.

Solid-state characterization

Single crystals of compounds **1–3**, suitable for X-rays analysis, were collected from ethyl acetate. In particular, suitable crystals of compounds **1**, **3** were obtained at room temperature by slow evaporation of the solvent; while those of compound **2**, after overnight cooling at 4 °C. A molecule of water was found in the elemental cell of compound **3** so that it will be indicated as **3**·H_2O hereinafter. In the crystal lattice of each of the compounds **1**, **2** and **3**·H_2O both enantiomers are present, as provided by the achiral space groups.

A comparison of the overall shape of the three molecules (see Fig. 5–7) shows that the tricyclic moieties of compounds **2** and **3** superimpose quite perfectly with the r.m.s. value, calculated using all the non-hydrogen atoms of the three rings, 0.10 Å. Both these compounds give a worse superimposition with **1** with r.m.s. value 0.26 Å for the **1–2** and the **1–3** couples.

In addition, in **1** and **3** the carboxylic chain shows a + synclinal conformation,[17] with a value of the dihedral angle C(7)–N(1)–C(14)–C(15) of 64.8(2) and 75.3(2)°, respectively, while in **2** it takes a −*syn*-clinal arrangement [C(7)–N(1)–C(14)–C(15) = −56.8(4)°].

Concerning the crystal packing, in all the three cases the hydrogen H_2O bound to O(2) strongly interacts *via* hydrogen bond with an oxygen atom provided by a symmetry related molecule [O(1)] in **1** and **2** and by a water molecule in **3**·H_2O. The bond distance and the bond angle defining the H-bond interaction are the same in all the three cases within 3σ (Table 1). Finally in **3**·H_2O there are two additional H-bond interactions where the crystallization water molecule acts as a H-bond donor (Table 1).

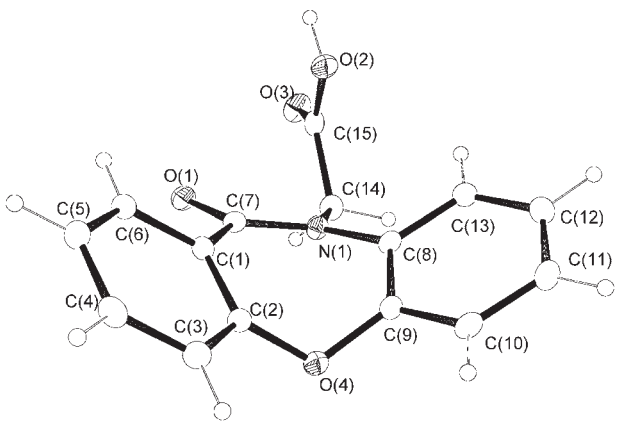

Fig. 5 ORTEP3 view of compound **1**. One of the two enantiomers present in the crystal lattice is represented.

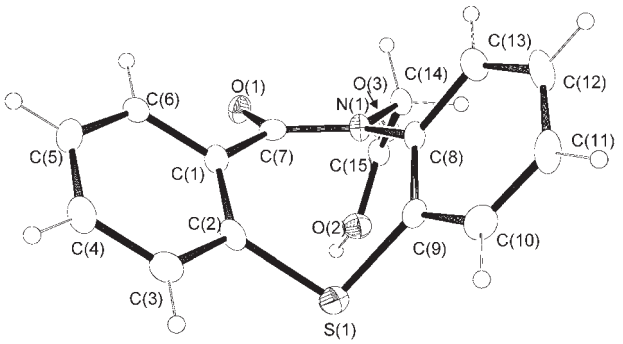

Fig. 6 ORTEP3 view of compound **2**. One of the two enantiomers present in the crystal lattice is represented.

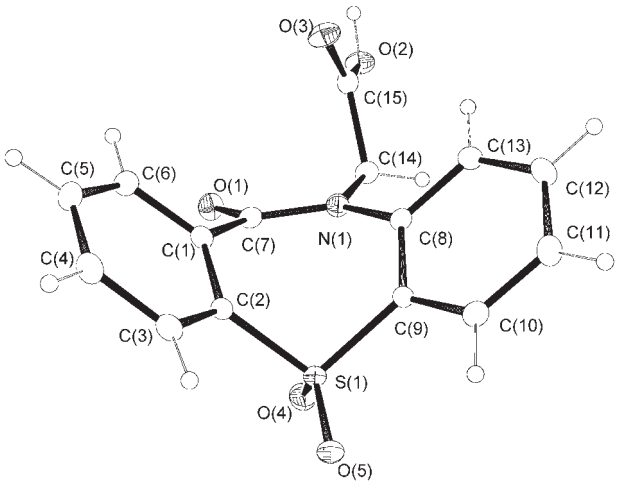

Fig. 7 ORTEP3 view of compound **3**. One of the two enantiomers present in the crystal lattice is represented.

Table 1 H-bond distances (Å) and angles (°) in compounds **1**, **2** and **3**·H_2O (D = donor, A = acceptor)

	D–H···A	*r*(D–H)	*θ*(D–H···A)
1	O(2)–H(2o)···O(1)[a]	1.82(3)	173(2)
2	O(2)–H(2o)···O(1)[b]	1.72(5)	170(5)
3·H_2O	O(2)–H(2o)···O(1w)[a]	1.74(3)	170(3)
	O(1w)–H(2w)···O(3)	1.88(3)	171(3)
	O(1w)–H(1w)···O(1)[c]	1.94(3)	172(3)

[a] = $-x, -y + 2, -z + 1$. [b] = $x - 1/2, -y - 1/2, +z$. [c] = $-x - 1, -y + 2, -z + 1$.

Molecular geometry: general considerations

The overall shape of the tricyclic model compounds **4–9** as well of **1**, **2** and **3** can be considered as the result of the conformation of the seven-membered ring and the folding of the two aromatic moieties about it.

Several geometrical parameters, obtained from *ab initio* geometry optimizations (details in the Experimental section), summed up in the following, have been monitored in order to check the role of the O → S → SO_2 substitution on the overall 3D arrangement of molecules **4–9** (Table 2). For comparison purposes the geometrical parameters as derived by X-ray data of **1**, **2** and **3**·H_2O have also been reported in Table 2.

For the conformation assumed by the seven-membered ring, the asymmetry index (ΔC_s)[18] and the bow and stern parameters[19] were considered in addition to the sum of the ring internal angles. The latter should be about 829° on the basis of the VSEPR rule.

Finally, also the geometry of the amide/thioamide grouping was checked, that is all the (S)O═CNMe bond distances, the sum of the angles about the amide nitrogen N(1) and the dihedral angle [S(2)]O(1)–C(7)–N(1)–C(14)[Me] (τ_1).

As an index of the folding of the two aromatic rings, the angle formed by each of them with the plane p_1 defined by C(7), N(1), O(4)[S(1)] was considered (τ_4).[20] Also the dihedral angles [Me]C(14)–N(1)–C(8)–C(13) (τ_2) and [S(2)]O(1)–C(7)–C(1)–C(6) (τ_3) were taken into account. Finally, the relative disposition of the two aromatic rings (A and B) was investigated by measuring the angle between their mean planes.

Ground states

The tricyclic skeleton geometry of the optimized model molecules (**4GS–6GS**, Fig. 8) well compares with those experimentally observed in the solid state for **1**, **2** and **3**·H_2O (Fig. 5–7).

Results concerning the molecules conformation can be summarized as follows:

(a) Amide/thioamide conjugation: no significant changes are observed in the series **4–9**. In fact in all the molecule ground states the nitrogen atom is trigonal planar, as provided by the summation of its three bond angles and by the τ_1 dihedral which remains close to 0° (Table 2). As a further comment, the C–N bond is significantly strengthened in thioamide rather than in amide derivatives as already found.[21]

(b) Seven-membered ring conformation: the optimized amide derivatives show a more evident deviation of the seven-membered ring from a pure boat conformation with respect to the thioamide ones (12.8° is the average value of the asymmetry index ΔC_s in **4GS–6GS** *vs.* 7.3° in **7GS–9GS**, 9.1 is the mean experimental value).

Bow and stern angular values show a less definite trend in the optimized molecules, as well in the experimental ones. As a final remark, the amide and thioamide derivatives **4GS**, **1** and **7GS** show the largest deviation from the ideal value (≈829°) of the seven-membered ring internal bond angles sum.

(c) Aromatic rings folding: both in amide and thioamide ground states (Fig. 8) moving from the oxygen to the sulfur derivatives increases the folding of the tricyclic ring system about the seven-membered ring, as provided by the τ_4 values (especially those referring to the A ring). Parallel increments are observed for the angle between the two phenyl ring mean planes (∠(A/B) values) and the torsion angles τ_2 and τ_3. Analogous trends can be recognized in the experimental structures. Thus the steric interactions between extra-annular atoms and/or groups (*e.g.* the C(7) carbonyl oxygen O(1)/sulfur S(2) with the hydrogen atom bound to C(6); the C(14) atom and the hydrogen atom on C(13)) lower on moving from O to S/SO_2 (Table 2).

These data suggest that the increased folding about the seven-membered ring, as observed along the O → S/SO_2 direction, causes a geometry relaxation of the molecule internal

Table 2 Most relevant geometrical parameters (distances (Å), angles (°)) as derived from *ab initio* geometry optimizations (HF/6-311G(d,p) level of theory) for the ground state (#**GS**) of the model compounds[a] and from X-ray diffraction for **1**, **2** and **3**·H_2O

	4GS	**5GS**	**6GS**	**7GS**	**8GS**	**9GS**	**1**	**2**	**3**·H_2O
r_{NC}/Å	1.369	1.368	1.369	1.341	1.338	1.342	1.362(2)	1.352(5)	1.374(2)
r_{CX}/Å	1.196	1.196	1.193	1.664	1.664	1.665	1.241(2)	1.239(5)	1.233(2)
r_{N-Me}/Å	1.460	1.462	1.466	1.467	1.468	1.470	1.466(2)	1.465(5)	1.470(3)
$\sum(\angle N)^b$/°	358.5	360.0	359.9	359.9	359.9	360.0	359.5	359.2	360.0
$\tau_1{}^c$/°	−4.2	−4.2	−7.7	−5.6	−4.9	−8.6	−2.2(2)	−1.0(5)	6.0(2)
$\tau_2{}^d$/°	36.0	46.9	49.1	46.3	57.1	58.9	35.2(2)	47.5(5)	38.2(2)
$\tau_3{}^e$/°	−24.4	−36.2	−36.5	−35.2	−48.0	−46.6	−29.4(2)	−40.1(5)	−45.7(2)
$\tau_4{}^f$/°	20.3/ 38.0	30.8/ 42.4	32.5/ 40.4	28.9/ 37.1	38.9/ 41.9	38.2/ 42.2	21.95(8)/ 34.07(8)	33.4(2)/ 39.93(2)	44.37(8)/ 30.03(7)
$\sum$internal $\angle{}^g$/°	845.4	831.7	836.3	837.4	823.5	828.4	847	833	835
$\angle$(A/B)^h/°	57.6	72.3	71.8	65.6	80.4	80.0	55.12(6)	72.6(1)	72.96(6)
$\Delta C_s{}^i$/°	15.1	13.0	10.3	8.3	6.3	7.4	9.6	9.9	7.7
Bow^i/°	53.8	50.1	49.9	55.3	50.7	49.6	53.6(1)	49.1(2)	52.35(7)
Stern^i/°	34.3	50.5	39.5	39.2	45.9	44.4	33.92(9)	42.1(2)	39.14(9)
O(1)[S(2)]···H(6)/Å	2.47	2.52	2.51	2.78	2.89	2.85	2.47(2)	2.625(3)	2.70(2)
C(14)···H(13)/Å	2.66	2.73	2.74	2.74	2.84	2.86	2.62(1)	2.724(4)	2.62(2)

[a] Refer to Fig. 4 for molecular models and atom labelling. [b] Summation of the bond angles about the amide nitrogen atom N(1). [c] [Me]C(14)–N(1)–C(7)–O(1)[S(2)] dihedral angle. [d] [Me]C(14)–N(1)–C(8)–C(13) dihedral angle. [e] [S(2)]O(1)–C(7)–C(1)–C(6) dihedral angle. [f] Angles between the plane through C(7),N(1),O(4)[S(1)] and the least-squares planes through rings A and B, respectively. [g] Sum of the internal bond angles in the seven-membered ring. [h] Interplanar angle between the aromatic rings. [i] See refs. 18 and 19 for the parameter definition.

degrees of freedom (seven-membered ring internal bond angles and steric interactions), thus contributing to stabilize the ground state equilibrium geometry of **5–6** *vs.* **4** and **8–9** *vs.* **7**.

Transition states

3D-views of the transition state structures (Fig. 9) evidence their "open" overall shape (especially for **4TS–8TS**) in contrast to the "folded" one featured by their corresponding ground states. The values of the angle comprised between the phenyl rings ($\angle$(A/B)) well quantify this aspect (Table 3). To this respect, it is noteworthy that the conformation of the central seven-membered ring, where the sum of the internal bond angles approaches 900° (the ideal value for an heptagon, see Table 3) largely contributes to the practically flat shape of **4TS** and **7TS**. In fact in **4TS** and **7TS** the amide/thioamide resonance, although weakened with respect to the corresponding **GS** (see r_{NC} and $\sum(\angle N)$ values in Table 3), is still active. On the contrary in the other **TS**s the atoms of the hepta-ring deviate significantly from planarity, as also evidenced by the structural parameters defining the amide/thioamide moiety (r_{NC}, $\sum(\angle N)$ and τ_1 in Table 3) which is not planar any more. The partial/total loss of amide resonance observed passing from the **GS**s to the **TS**s should in part contribute to cut off strong steric interactions between extra-annular substituents due to the flatter shape of the transition state equilibrium geometries with respect to the corresponding **GS** (which however are not so dramatically important in **4TS** and **7TS**).

Thus it appears that reaching the transition states for the sulfide/sulfone derivatives (**5–6**, **8–9**) implies the breaking of

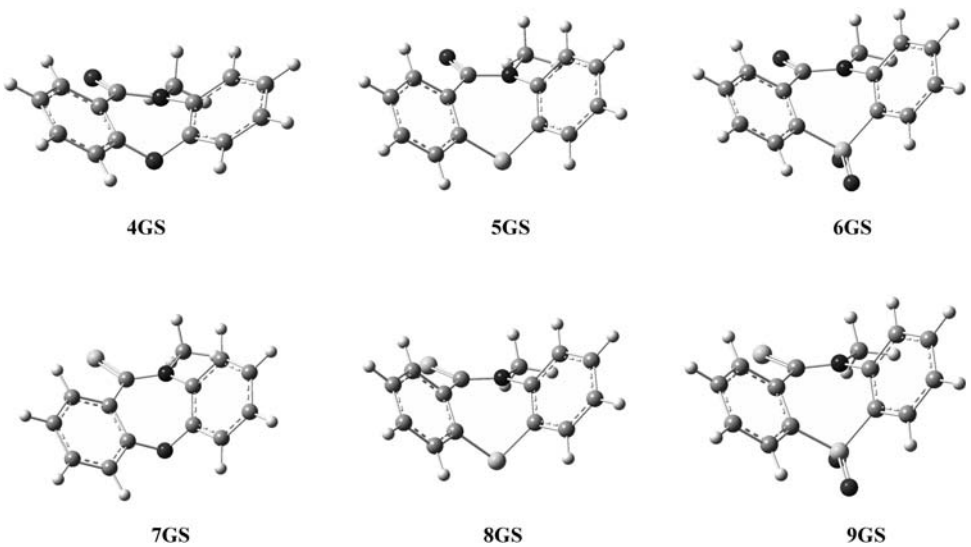

Fig. 8 Optimized ground state of the model compounds **4–9** (HF/6-311G(d,p) level of theory).

the partial double character of the C–N oxo/thio–amide bond, which, however, should be in part energy balanced by the removal of the steric interactions between extra-annular appendages.

Electronic structures

To get an electronic picture of the model compounds **4–9** the Weinhold's Natural Bond Orbital (NBO) analysis[22] has been used. Thanks to this method, together with Natural Resonance Theory (NRT),[23] Glendening and co-workers[21] accounted for the fact that oxoamides have smaller rotational barrier than the corresponding thioamides. This experimental evidence, which appears counterintuitive on the basis of the relative O/S electronegativities, has been explained by considering that the amide resonance and, as a consequence, the contribution of the dipolar form $N^{+}{=}CX^{-}$ increases from formamide to telluroamide (X = O, S, Se, Te). The reason supplied by Glendening on the basis of NBO and NRT theories is that the larger is the polarizability of the chalcogen, the better it lodges additional charge density, thus enhancing the resonance stabilization.

According with the Glendening paper, the twisting about τ_1 which accompanies the **GS** → **TS** path in **4–9**, causes an elongation of the CN bond and a contraction (less evident) of the CX one, thus suggesting that similar electronic effects are involved in our tricyclic systems. Actually within each model compound, the variation of natural charges (Natural Population Analysis, NPA) on N(1), C(7), O(1)[(S2)] on going from #**GS** to #**TS** is consistent with that expected on the basis of the resonance picture (O(S) → N charge transfer). In addition the overall shifted charge (*osc*, hereafter) is invariably larger in the thioamide family than in the oxoamide one, thus supporting that the resonance stabilization increases from oxo to thioamide derivatives. Finally, on the basis of the *osc*, we can assume that the contribution of the dipolar form increases within each family (*e.g.* **4** → **6** and **7** → **9**).

Inversion barriers

In Table 4 the inversion barriers calculated for the model compounds **4–9** are reported. The analysis of the results evidenced that within each series (oxo/thio-derivatives) the inversion barrier increases moving from the O to the $S(SO_2)$ compounds (*e.g.* **5**/**6** *vs.* **4** and **8**/**9** *vs.* **7**). Concerning homologous molecules, thioamides appear on the whole characterized by a larger inversion barrier with respect to the corresponding amides (with the exception of the **6**/**9** couple).

NMR spectroscopy

Solution studies were performed on compounds **12** (Scheme 1) and **2** by means of ^{1}H DNMR, using the coalescence temperature method and choosing as probe the AB system of the methylene group in alpha position to the amidic nitrogen ($\delta \approx 4$ ppm).

The rate constant at the coalescence temperature of the signals, T_c, was derived using the approximate relation

$$k_c = \frac{\pi}{\sqrt{2}}\sqrt{(\nu_A - \nu_B)^2 + 6J_{AB}{}^2}$$

The Gibbs free energy of activation for the ring inversion process was evaluated with the Eyring equation.

$$\Delta G^{\ddagger} = RT[23.76 - \ln(k/T)]$$

It must be pointed out that the activation entropy of this kind of processes is usually close to zero and therefore negligible; for this reason, the comparison of barriers measured at different coalescence temperatures can be considered meaningful.[24]

Fig. 10 displays the behaviour of the methylene group signals in the ^{1}H NMR spectra of compound **12**, acquired at different temperatures in CD_2Cl_2 solution. At room temperature the two protons give rise to a broad singlet, indicating that in such conditions the ring inversion rate is fast on the NMR timescale. Upon cooling, coalescence of the signal occurred at 257 K, allowing us to calculate a barrier of 11.5 kcal mol^{-1} expressed as the Gibbs free energy of activation.

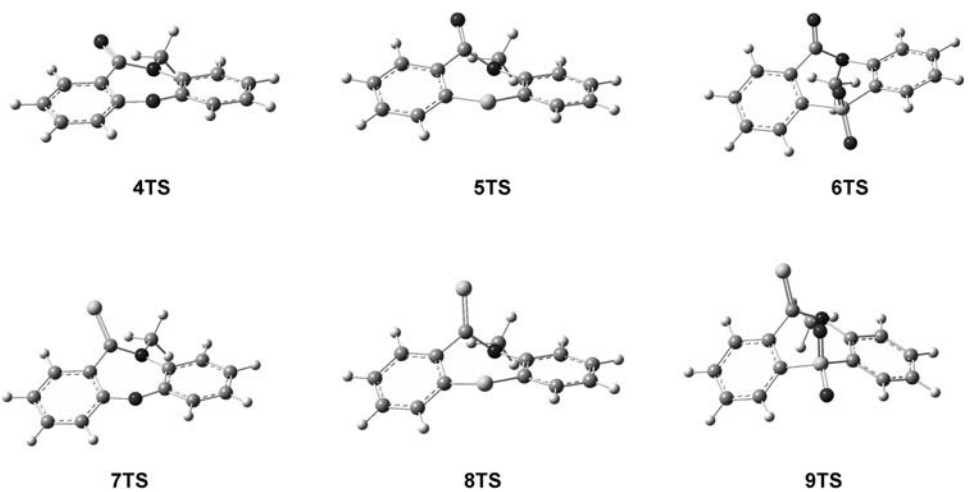

Fig. 9 Optimized transition state of the model compounds **4–9** (HF/6-311G(d,p) level of theory).

Table 3 Most relevant geometrical parameters (distances (Å), angles (°)) as derived from *ab initio* geometry optimizations (HF/6-311G(d,p) level of theory) for the transition states (#**TS**) of the model compounds[a]

	4TS	**5TS**	**6TS**	**7TS**	**8TS**	**9TS**
r_{NC}/Å	1.384	1.416	1.412	1.382	1.428	1.430
r_{CX}/Å	1.194	1.184	1.177	1.641	1.608	1.598
r_{N-Me}/Å	1.464	1.462	1.462	1.462	1.455	1.471
$\sum(\angle N)^b$/°	358.7	352.5	348.9	356.0	351.8	352.4
$\tau_1{}^c$/°	−15.0	−33.7	−141.8	−29.8	−60.5	−94.3
$\tau_2{}^d$/°	6.5	10.3	90.8	11.5	12.1	49.3
$\tau_3{}^e$/°	18.7	35.1	60.0	35.8	58.8	62.6
$\tau_4{}^f$/°	25.0/15.3	47.0/33.7	56.7/48.5	39.6/28.1	61.0/38.4	60.7/12.2
$\sum$internal $\angle{}^g$/°	889.8	861.1	836.7	875.6	836.4	838.2
$\angle(A/B)^h$/°	12.8	22.6	27.2	19.4	31.2	48.8
$\Delta C_s{}^i$/°	30.0	60.8	77.3	47.8	55.6	54.7
Bow^i/°	16.7	20.6	17.5	18.5	28.5	45.2
Stern^i/°	5.4	8.5	9.9	7.9	16.8	26.9
O(1)[S(2)]···H(6)/Å)	2.30	2.46	2.94	2.67	3.10	3.14
C(14)···H(13)/Å	2.34	2.37	3.31	2.36	2.46	2.67

[a] Refer to Fig. 4 for molecular models and atom labelling. [b] Summation of the bond angles about the amide nitrogen atom N(1). [c] [Me]C(14)–N(1)–C(7)–O(1)[S(2)] dihedral angle. [d] [Me]C(14)–N(1)–C(8)–C(13) dihedral angle. [e] [S(2)]O(1)–C(7)–C(1)–C(6) dihedral angle. [f] Angles between the plane through C(7),N(1),O(4)[S(1)] and the least-squares planes through rings A and B, respectively. [g] Sum of the internal bond angles in the seven-membered ring. [h] Interplanar angle between the aromatic rings. [i] See refs. 18 and 19 for the parameter definition.

Finally, in the slow motion limit (220 K), the AB system given by the CH_2 moiety is an indication that the ring inversion motion was successfully frozen.

The aliphatic part of compounds **13** and **14** spectra, acquired at room temperature, is quite similar to the one observed for compound **12** in the slow motion limit, a clear hint of higher inversion barrier and VT experiments performed on compound **2** (corresponding carboxylic acid of compound **13**) evidenced that the net effect upon heating up to 343 K was just a slight broadening of the CH_2 AB system. Unfortunately, since our NMR facility did not allow higher temperatures, the inversion barrier was obtained as a minimum threshold value of 16 kcal mol^{-1}.

A simulation performed on **2**, **13** and **3**, **14** using the values of $\delta\nu$ and J from their RT ^{1}H NMR spectra, and the calculated inversion barriers of their homologous model compounds (**5** and **6**, respectively), yielded a coalescence temperature of about 470 K for **2**, **12** and of 538 K for **3**, **13**.

Final remarks

The theoretical and experimental energetic trends (*ab initio* and NMR results) found in the racemisation barriers of the studied molecules can be rationalized on the basis of the structural features (both geometrical and electronic) of the model compounds. For example, within each lactam and thiolactam series (**4** → **6** and **7** → **9**, respectively) the larger deviation from the ideal internal bond angle values of the seven-membered ring of the oxo derivatives suggest that their **GS**s are affected by a greater strain with respect to those of the S/SO_2 ones. At the same time they should reach their corresponding **TS**s more easily with respect to the other model compounds given that they do not necessitate energy to disrupt the amide resonance. As a consequence the oxo species **4**, **7** and **12**, should have an inversion barrier smaller than the analogous heavier molecules. Finally NPA results, which evidence that the weight of resonance in stabilizing the **GS** equilibrium structures increases on moving from oxoamide to thioamide molecules, account for the observed trend in the racemisation barrier for each homologous couple **4**/**7**, **5**/**8**, **6**/**9**.

Table 4 HF/6-311G(d,p)// HF/6-311G(d,p)-Calculated inversion barriers (kcal mol^{-1}) for the model compounds

	ΔE(TS-GS)[a]	ΔE(TS-GS)[b]	ΔE(TS-GS)[c]	ΔG(TS-GS)[d]
4	13.3	13.2	12.8	13.8
5	21.3	21.1	20.6	21.7
6	26.1	25.2	24.9	25.7
7	18.1	17.7	17.3	18.3
8	24.0	23.3	22.9	23.7
9	25.1	24.2	23.6	23.9

[a] Calculated from electronic energies. [b] Calculated from electronic energies corrected by ZPVE. [c] Calculated from electronic energies including the thermal energies at 298 K. [d] Calculated from electronic energies including the Gibbs energy correction at 298 K.

Conclusion

Results from *ab initio* and NMR studies both agree in suggesting that the ring inversion of the oxo derivatives (**4**, **7** and **12**) is easier with respect to the corresponding S/SO_2 derivatives (Table 4). Also amide derivatives have, on the whole, smaller barriers with respect to the corresponding thioamide ones. Thus, a change in the nature of the group "X" (O → S → SO_2), as well as hopping from the oxo- to the thio-amide grouping, reduces the flexibility of the corresponding tricyclic ring, though not enough to allow a facile handling of the enantiomers at room temperature. Compounds to which

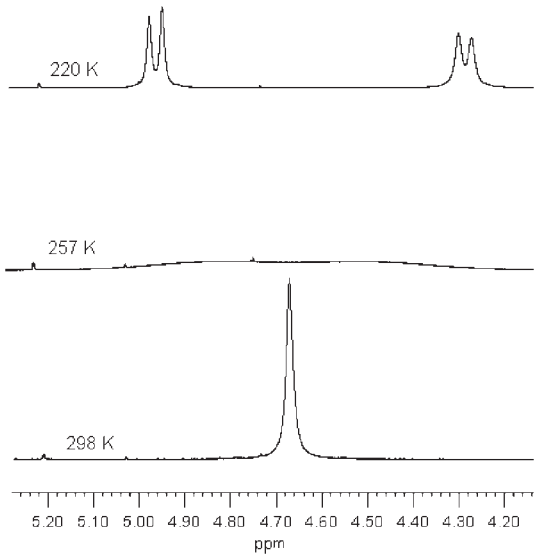

Fig. 10 Dynamic behaviour of the methylene group signals of compound **12**.

the findings disclosed in this paper can be reasonably extended, appeared recently in the patent literature.[25]

Experimental

General remarks

Anhydrous solvents were purchased from Fluka. TLC monitoring: Merck silica gel 60 F_{254} plates, detection by UV light. Melting points were measured in capillary tubes with a digital electrothermal apparatus Büchi B-540 and were uncorrected. IR spectra were collected with a Nicolet Avatar 360 FT-IR E.S.P. spectrophotometer, equipped with ATR Smart MIRacle sampler. Spectra were ATR corrected using the module present in the spectrophotometer software. ^{1}H NMR spectra were acquired at 600 MHz on a Bruker AC 600 spectrometer and referenced against the residual solvent peak ([D_6]DMSO at 2.50 ppm, CD_2Cl_2 at 5.31 ppm and $CDCl_3$ at 7.25 ppm). For variable-temperature studies, the probe temperature was calibrated by means of a 40% methanol standard. In dependence on the examined temperature range, either CD_2Cl_2 or DMSO d_6 were chosen as solvents, in the approximation that a change in solvent would affect negligibly the $\Delta G^{\ddagger}$ of activation. Spectra were referenced on residual solvent. ^{13}C NMR spectra were acquired on a Varian Gemini 200 spectrometer, at the operating frequency of 50 MHz and referenced against the residual solvent peak ([D_6]-DMSO at 39.43 ppm and $CDCl_3$ at 77.00 ppm). All processings were performed using the software *Mestrec 4.5.9.1*. Mass spectra were obtained with a Finnigan LCQ ion trap mass spectrometer, operated in positive-ion electrospray ionization. The samples were analyzed by full-scan MS and product ion MS/MS of the protonated quasi-molecular ions, at 30% relative collision energy, using helium as the collision gas. The high resolution mass spectra were obtained with a Micromass Q-Tof micro mass spectrometer, calibrated with 0.1% phosphoric acid in 1 : 1 H_2O–MeCN. This same mixture was used also as internal reference compound during ESI-MS accurate mass experiments, and was introduced *via* the LockSpray channel using an infusion pump. Ionization mode: ESI, positive ion. Scan mode: Full-scan MS from m/z 100 to 1000. Capillary voltage: 3300 V; Capillary temperature: 150 °C; Source temperature: 80 °C. Cone gas: nitrogen, 50 L h^{-1}. Desolvation gas: nitrogen, 650 L h^{-1}. Sample introduction: direct infusion through the built-in syringe pump, flow 5 mL min^{-1}.

Synthesis and characterization of compounds 1–3

(11-Oxo-11*H*-dibenzo[*b*,*f*][1,4]oxazepin-10-yl)acetic acid methyl ester 12. Compound **10** (425 mg, 2.01 mmol) was dissolved in 15 mL of dried DMF. Under an inert atmosphere of N_2, NaH (135 mg of 60% dispersion in mineral oil, *ca.* 3.40 mmol) was added in one portion into the reaction flask. The mixture was stirred for 10 min at 70 °C. A homogeneous, pale yellow solution was observed. Then, methyl bromoacetate (310 µl, *ca.* 3.40 mmol) was added and the reaction mixture stirred for 3 h at 70 °C. At room temperature, the solution was poured slowly onto ice (*ca.* 60 g) and the resulting white mixture was stirred vigorously for 10 min, before extraction by ethyl acetate (3 × 40 ml). The combined organic phases were dried over anhydrous Na_2SO_4, filtered and concentrated under reduced pressure. The residue was purified by Flash-Master chromatography. The apolar products were eluted using 20% of cyclohexane in CH_2Cl_2. Compound **12** was eluted while decreasing progressively to zero the proportion of cyclohexane (520 mg as a white solid; yield = 91%). Mp 109–110 °C. R_f ($CHCl_3$) = 0.2. ^{1}H NMR (CD_2Cl_2, 600 MHz): δ 3.87 (s, 3H), 4.67 (br s, 2H) 7.20–7.30 (m, 5H), 7.32–7.36 (m, 1H), 7.52–7.56 (m, 1H), 7.85–7.87 (m, 1H). ^{13}C NMR ($CDCl_3$, 50 MHz): 51.67t, 52.22q, 119.70d, 121.26d, 122.25d, 125.05d, 125.46s, 125.80d, 126.51d, 132.07d, 133.63d, 134.88s, 153.35s, 160.40s, 166.18s, 169.29s. IR (cm^{-1}): 3068, 3027, 2986, 2945, 1748, 1645, 1605, 1497, 1452, 1415, 1375, 1210. ESI$^+$-MS: m/z = 284 (MH^+); 252; 224. HRMS: 284.0928 ([$C_{16}H_{13}NO_4$ + H]$^+$; calc. 284.0923).

(11-Oxo-11*H*-dibenzo[*b*,*f*][1,4]oxazepin-10-yl)acetic acid 1. Compound **12** (200 mg, 0.71 mmol) was dissolved in 30 mL of MeOH. Methanolic KOH (0.40 g, 7.1 mmol, dissolved in 20 mL of MeOH) was added and the mixture was refluxed for 3 h. The solvent was removed under reduced pressure and the residue (white solid) dissolved into 35 mL of distilled water. At 0 °C, HCl (1 M solution) was added dropwise until pH = 1. The white precipitate was filtered off under reduced pressure and washed with 100 mL of water. This material was dissolved in 10 mL of ethyl acetate and the solution dried over anhydrous Na_2SO_4. After filtration, concentration and drying under vacuum provided compound **1** as a white solid (130 mg, yield = 68%). Mp 204–206 °C. ^{1}H NMR (DMSO-d_6, 600 MHz): δ 4.65 (s, 2H), 7.26–7.29 (m, 2H), 7.30–7.33 (m, 1H), 7.35–7.40 (m, 3H), 7.58–7.62 (m, 1H), 7.71–7.73 (m, 1H), 13.10 (br s, 1H). ^{13}C NMR (DMSO-d_6, 50 MHz): δ 51.26t, 119.94d, 121.12d, 122.91d, 125.46d, 126.12d, 126.57d, 131.58d, 134.11d, 134.58s, 152.82s, 159.93s, 165.21s, 170.03s. ESI$^+$-MS: m/z = 270.1 (MH^+). HRMS: 270.0764 ([$C_{15}H_{11}NO_4$ + H]$^+$; calc. 270.0766).

(11-Oxo-11*H*-dibenzo[*b*,*f*][1,4]thiazepin-10-yl)acetic acid methyl ester 13. Compound **11** (15.0 g, 66.1 mmol) was dissolved in 360 mL of dry DMF, under nitrogen atmosphere. NaH (3.96 g of 60% dispersion in mineral oil, 99.1 mmol) was added in one portion into the reaction flask. The mixture was stirred for 10 min at 60 °C. A yellowish solution was obtained. Methyl bromoacetate (9.1 mL, 99.1 mmol) was added and the reaction mixture stirred at 80 °C for 5 h. At room temperature, the solution was poured slowly into a magnetically stirred ice/water mixture (*ca.* 300 mL). The resulting heterogeneous mixture was stirred vigorously for 10 min and filtered. The solid material was washed with 500 mL of water and re-dissolved in 100 mL of anhydrous toluene. After drying over Na_2SO_4 and filtration, toluene was removed by rotovapor distillation. The dissolution in anhydrous toluene (50 ml) and rotovapor distillation was repeated four times to obtain compound **13** as a yellow solid (15.6 g, yield = 79%). Mp 120–123 °C. ^{1}H NMR ($CDCl_3$, 600 MHz): δ 3.87 (s, 3H), 4.31 and 4.97 (AB system, ^2J = 17.1 Hz, 2H), 7.10–7.15 (m, 1H), 7.30–7.33 (m, 3H), 7.41–7.46 (m, 2H), 7.59–7.60 (m, 1H), 7.73–7.75 (m, 1H). ^{13}C NMR ($CDCl_3$, 50 MHz): δ 52.33q, 53.65t, 124.39d, 126.48d, 128.45d, 129.72d, 130.89d, 131.09d, 131.69d, 33.00d, 134.66s, 137.23s, 138.61s, 143.96s, 168.83s, 169.53s. IR (cm^{-1}): 2951, 2922, 2844, 1741, 1640, 1581, 1474, 1432, 1380, 1317, 1210. ESI$^+$-MS: m/z = 300 (MH^+), 268, 240. HRMS: 300.0696 ($[C_{16}H_{13}NO_3S + H]^+$; calc. 300.0694).

(11-Oxo-11*H*-dibenzo[*b*,*f*][1,4]thiazepin-10-yl)acetic acid 2. Compound **13** (5.0 g, 16.7 mmol) was dissolved in 300 mL of warm MeOH (50 °C). Methanolic KOH (9.4 g, 167 mmol dissolved in 20 mL of MeOH) was added and the mixture was refluxed for 3 h. The solvent was removed under reduced pressure and the white solid residue was dissolved in 200 mL of water. At 0 °C, aqueous HCl (37%) was added dropwise until pH 1. A white solid separated, which was filtered off, washed with 500 mL of distilled water and recrystallised from ethyl acetate. Compound **2** was obtained as a white solid (3.7 g, yield = 78%). Mp 195–196 °C. ^{1}H NMR (DMSO-d_6, 600 MHz): δ 4.44 and 4.73 (AB system, ^2J = 17.1 Hz, 2H), 7.21–7.24 (m, 1H), 7.41–7.46 (m, 3H), 7.51–7.55 (m, 2H), 7.59–7.61 (m, 1H), 7.63–7.65 (m, 1H), 13.01 (br s, 1H). ^{13}C NMR (DMSO-d_6, 50 MHz): δ 53.25t, 124.73d, 126.44d, 128.76d, 130.16d, 130.83d, 131.20d, 131.38d, 132.76d, 133.45s, 137.22s, 137.87s, 143.53s, 167.69s, 170.06s. ESI$^+$-MS: m/z = 286. (MH^+) 268, 240. HRMS: 286.0538 ($[C_{15}H_{11}NO_3S + H]^+$; calc. 186.0538).

(5,5,11-Trioxo-5,11-dihydro-5λ^6-dibenzo[*b*,*f*][1,4]thiazepin-10-yl)acetic acid methyl ester 14. Compound **13** (3.0 g, 10.0 mmol) was dissolved in 70 mL of CH_2Cl_2. *m*CPBA (9.0 g, 40 mmol, dissolved in 50 mL of CH_2Cl_2) was added and the reaction mixture stirred at RT for 3 h. $NaHSO_3$ (10% aqueous solution, 150 mL) was added under magnetic stirring. The aqueous layer was separated off and the organic phase was washed first with aqueous NaOH (1 M, 150 mL) and then with water (2 × 200 mL). The resulting organic phase was dried over anhydrous Na_2SO_4 and the volatiles removed under reduced pressure. Recrystallization from H_2O–MeOH provided compound **14** as a white solid. (2.9 g, yield = 88%). Mp 198–199 °C; R_f(5% v/v ethyl acetate in CH_2Cl_2) = 0.43. ^{1}H NMR (DMSO-d_6, 600 MHz): δ 3.81 (s, 3H), 4.68 and 4.85 (AB system, ^2J = 17.2 Hz, 2H), 7.52–7.56 (m, 1H), 7.62–7.66 (m, 1H), 7.79–7.86 (m, 4H), 7.92–7.94 (m 1H), 7.97–7.99 (m, 1H). ^{13}C NMR ($CDCl_3$, 50 MHz): δ 52.67q, 54.31t, 123.85d, 125.29d, 126.75d, 126.78d, 130.51s, 131.67d, 132.51d, 133.88d, 134.63d, 136.84s, 140.10s, 141.72s, 166.58s, 169,62s. IR (cm^{-1}): 2989, 2951, 2924, 2852, 1737, 1647, 1590, 1572, 1433, 1368, 1327, 1236, 1218, 1172, 1127. ESI$^+$-MS: m/z = 332 (MH^+), 300, 272. HRMS: 332.0599 ($[C_{16}H_{13}NO_5S + H]^+$; calc. 332.0605).

(5,5,11-Trioxo-5,11-dihydro-5λ^6-dibenzo[*b*,*f*][1,4]thiazepin-10-yl)acetic acid 3. Compound **14** (1.40 g, 4.20 mmol) was dissolved in 70 mL of MeOH and the solution was heated at 50 °C. Aqueous KOH (2.37 g, 42.3 mmol, pre-dissolved in 50 mL of water) was added and the mixture was refluxed for 3 h. The solvent was removed under reduced pressure and the residue (white solid) was dissolved into 50 mL of distilled water. At 0 °C, aqueous HCl (37%) was added dropwise until pH 1. Extraction was performed by ethyl acetate (4 × 50 mL). The combined organic phases were dried over anhydrous Na_2SO_4 and the volatiles removed under reduced pressure. Compound **3** was obtained as a white solid (1.05 g, yield = 78%). Mp 112–113 °C. ^{1}H NMR (DMSO-d_6, 600 MHz): δ 4.49 and 4.78 (AB system, ^2J = 17.3 Hz, 2H), 7.51–7.55 (m, 1H), 7.63–7.65 (m, 1H), 7.77–7.87 (m, 4H), 7.91–7.93 (m, 1H), 7.96–7.98 (m, 1H), 13.23 (br s, 1H). ^{13}C NMR ($CDCl_3$, 50 MHz): δ 54.44t, 123.94d, 126.27d, 126.71d, 127.98d, 130.55s, 132.63d, 133.22d, 135.22d, 136.04s, 136.28d, 139.81s, 141.37s, 167.10s, 170.94s ESI$^+$-MS: m/z = 318 (MH^+), 300, 272. HRMS: 318.0436 ($[C_{15}H_{11}NO_5S + H]^+$; calc. 318.0436).

Crystal data and refinement

For compounds **1**, **2** and **3**·H_2O intensity data were collected on an Oxford Diffraction Xcalibur diffractometer equipped with a CCD area detector, using Mo-Kα radiation (0.71069 Å) for compound **1** and **3**·H_2O and Cu-Kα radiation (1.54018 Å) for compound **2**, monochromated with a graphite prism. Data were collected through the program CrysAlis CCD[26] and the reduction was carried on with the program CrysAlis RED.[27] Absorption correction was performed with the program ABSPACK in CrysAlis RED. Structures were solved with the direct methods of the SIR97[28] package and refined by full-matrix least squares against F^2 with the program SHELX97.[29]

All the non-hydrogen atoms were refined anisotropically. All the hydrogen atoms of compound **1** and **3**·H_2O, as well as the hydrogen bonded to O(2) [H(2o)] in compound **2**, were found in the Fourier difference map and refined isotropically, all the other hydrogen atoms of compound **2** were set in calculated positions and refined in agreement with the atoms to which they are bound.

Geometrical calculations were performed by PARST97[30] and molecular plots were produced by the program ORTEP3.[31]

Crystallographic data and refinement parameters for compounds **1**, **2** and **3**·H_2O are reported in Table 5.

Table 5 Crystallographic data and refinement parameters for **1**, **2** and **3**·H_2O

	1	**2**	**3**·H_2O
Chemical formula	$C_{15}H_{11}NO_4$	$C_{15}H_{11}NO_3S$	$[C_{15}H_{11}NO_5S]^{\bullet}H_2O$
M	269.25	285.31	335.32
T/K	150	150	150
λ/Å	0.71069	1.54018	0.71069
Crystal system	Triclinic	Monoclinic	Triclinic
Space group	$P\bar{1}$	$P2_1/a$	$P\bar{1}$
a/Å	7.553(1)	7.7680(9)	8.117(1)
b/Å	8.305(2)	11.736(1)	8.432(1)
c/Å	10.514(2)	14.923(2)	11.705(2)
α/°	68.89(2)		108.32(1)
β/°	80.78(1)	104.66(1)	90.98(1)
γ/°	75.12(2)		99.13(1)
V/Å^3	592.9(2)	1316.2(3)	749.0(2)
Z, D_c/g cm^{-3}	2, 1.508	4, 1.440	2, 1.487
μ/mm^{-1}	0.111	2.252	0.248
Reflections collected/unique	6833/2599	8125/2871	9073/3290
R_{int}	0.0303	0.0701	0.0206
Data/parameters	2599/225	2871/185	3290/260
Final R indices [$I > 2\sigma(I)$]	$R1 = 0.0416$, $wR_2 = 0.0848$	$R1 = 0.0555$, $wR_2 = 0.1117$	$R1 = 0.0403$, $wR_2 = 0.1099$
R indices (all data)	$R1 = 0.0737$, $wR_2 = 0.0943$	$R1 = 0.1361$, $wR_2 = 0.1194$	$R1 = 0.0495$, $wR_2 = 0.1181$

Refinement method: full-matrix least-squares on F^2

Computational study

The GAUSSIAN03 (Revision B.05)[32] package implemented on a personal computer was used for the computational studies. Model compounds (**4–9**) are sketched in Fig. 4. In all cases the level of theory was HF-SCF, the basis set were 6-311G(d,p)[33] and 6-311+G(d,p).[34] Results from the two model chemistry are not significantly different either in the geometrical parameters and in the energetic trends. The starting geometry of the molecule ground states (#**GS**) was derived from the solid-state structures. The reliability of the stationary points was assessed by the evaluation of the vibrational frequencies. Transition structures for the enantiomers interconversion (#**TS**) were located with the SQTN method (QST2 and QST3 keywords) or with the Berny algorithm[35] (OPT = TS). In all cases the normal mode corresponding to the imaginary frequency was checked in order to test their reliability. NBO analyses were performed using the NBO 5.0 program.[22]

Acknowledgements

We thank CRIST (Centro Interdipartimentale di Cristallografia Strutturale, University of Florence), Dr Samuele Ciattini for X-ray data collection, and Dr Antonio Triolo for performing mass spectra.

References

1 P. Dapporto, A. Guerri, P. Paoli, P. Rossi, M. Altamura, F. R. Calabri and A. Guidi, *J. Mol. Struct. (THEOCHEM)*, 2002, **617**, 189.
2 M. Altamura, F. Canfarini, R.-M. Catalioto, A. Guidi, F. Pasqui, A. R. Renzetti, A. Triolo and C. A. Maggi, *Bioorg. Med. Chem. Lett*., 2002, **12**, 2945.
3 M. Altamura, G. Coppini, F. Cuda, P. Dapporto, A. Guerri, A. Guidi, C. Nativi, P. Paoli and P. Rossi, *J. Mol. Struct*., 2005, **749**, 20.
4 M. Reist, B. Testa, P.-A. Carrupt, M. Jung and V. Schurig, *Chirality*, 1995, **7**, 396.
5 M. Altamura, G. Balacco, F. Cuda, A. Guerri, A. Guidi, S. Meini, S. Menichetti, C. Nativi and F. Pasqui, *Tetrahedron*, 2006, **62**, 6754.
6 J. Cossy, C. Dumas and D. Gomez Pardo, *Eur. J. Org. Chem*., 1999, 1693.
7 D. Giannotti, G. Viti, P. Sbraci, V. Pestellini, G. Volterra, F. Borsini, A. Lecci, A. Meli, P. Dapporto and P. Paoli, *J. Med. Chem*., 1991, **34**, 1356.
8 A. Ebnöther, E. Junker and A. Stoll, *Helv. Chim. Acta*, 1965, **48**, 1237.
9 24 M. Nogradi, W. D. Ollis and I. O. Sutherland, *Chem. Commun*., 1970, 158.
10 D. C. Remy, K. E. Rittle, C. A. Hunt, P. S. Anderson, E. L. Engelhardt, B. V. Clineschmidt and A. Scriabine, *J. Med. Chem*., 1977, **20**, 1681.
11 Å. Lundquist and J. Sandström, *Chem. Scr*., 1974, **5**, 52.
12 M. Eltze, *Eur. J. Pharmacol*., 1990, **180**, 161.
13 K. M. J. Brands and A. J. Davies, *Chem. Rev*., 2006, **106** 2711.
14 J. Irurre, F. Marquillas, A. Alvarez-larena and J. F. Piniella, *Can. J. Chem*., 1994, **72**, 334.
15 (*a*) P. Linscheid and J.-M. Lehn, *Bull. Chim. Sic. Fr*., 1967, 992; (*b*) N. W. Gilman, P. Rosen, J. V. Earley, C. Cook and J. L. Todaro, *J. Am. Chem. Soc*., 1990, **112**, 3969; (*c*) P. C.-H. Lam and P. R. Carlier, *J. Org. Chem*., 2005, **70**, 1530.
16 B. Paizs and M. Simonyi, *Chirality*, 1999, **11**, 651.
17 W. Klyne and V. Prelog, *Experientia*, 1960, **16**, 521.
18 W. L. Duax, C. M. Weeks and D. C. Rohrer, in *Topics in Stereochemistry*, ed. E. L. Eliel and N. Allinger, John Wiley & Sons, New York, 1976, vol. 9, p. 271.
19 V. Bertolasi, V. Ferretti, G. Gilli and P. A. Borea, *Cryst. Struct. Commun*., 1982, **11**, 1481.
20 R. Usha, M. M. Bhadbhade, K. Venkatesan, K. Nagarajan and J. David, *Acta Crystallogr., Sect. B*, 1982, **38**, 1854.
21 E. D. Glendening and J. A. Hrabal II, *J.Am. Chem. Soc*., 1997, **119**, 12940.
22 E. D. Glendening, J. K. Badenhoop, A. E. Reed, J. E. Carpenter, J. A. Bohmann, C. M. Morales and F. Weinhold, *NBO 5.0*., Theoretical Chemical Institute, University of Wisconsin Madison, 2001.
23 (*a*) E. D. Glendening, PhD Thesis, University of Wisconsin, Madison, WI, 1991; (*b*) E. D. Glendening and F. Weinhold, *J. Comput. Chem*., 1998, **19**, 610.
24 Ma. B. Garcia, S. Grilli, L. Lunazzi, A. Mazzanti and L. R. Orelli, *J. Org. Chem*., 2001, **66**, 6679.
25 A. Guidi, T. Dimoulas, D. Giannotti and N. J. S. Harmat, *World Pat*., WO 2006097449, 2006A. Guidi, T. Dimoulas, D. Giannotti and N. J. S. Harmat, *Chem. Abstr*., 2006, **145**, 356813.

26 CrysAlis CCD, Oxford Diffraction Ltd., Version 1.171.29.2 (release 20.01.2006 CrysAlis171.NET).
27 CrysAlis RED, Oxford Diffraction Ltd., Version 1.171.29.2 (release 20.01.2006 CrysAlis171.NET).
28 A. Altomare, G. L. Cascarano, C. Giacovazzo, A. Guagliardi, A. G. Moliterni, M. C. Burla, G. Polidori, M. Camalli and R. Spagna, *J. Appl. Crystallogr.*, 1999, **32**, 115.
29 G. M. Sheldrick, *SHELX97*, University of Göttingen, Germany, 1997.
30 M. Nardelli, *J. Appl. Crystallogr.*, 1995, **28**, 659.
31 L. J. Farrugia, *J. Appl. Crystallogr.*, 1997, **30**, 565.
32 M. J. Frisch, G. W. Trucks, H. B. Schlegel, G. E. Scuseria, M. A. Robb, J. R. Cheeseman, Jr, J. A. Montgomery, T. Vreven, K. N. Kudin, J. C. Burant, J. M. Millam, S. S. Iyengar, J. Tomasi, V. Barone, B. Mennucci, M. Cossi, G. Scalmani, N. Rega, G. A. Petersson, H. Nakatsuji, M. Hada, M. Ehara, K. Toyota, R. Fukuda, J. Hasegawa, M. Ishida, T. Nakajima, Y. Honda, O. Kitao, H. Nakai, M. Klene, X. Li, J. E. Knox, H. P. Hratchian, J. B. Cross, C. Adamo, J. Jaramillo, R. Gomperts, R. E. Stratmann, O. Yazyev, A. J. Austin, R. Cammi, C. Pomelli, J. W. Ochterski, P. Y. Ayala, K. Morokuma, G. A. Voth, P. Salvador, J. J. Dannenberg, V. G. Zakrzewski, S. Dapprich, A. D. Daniels, M. C. Strain, O. Farkas, D. K. Malick, A. D. Rabuck, K. Raghavachari, J. B. Foresman, J. V. Ortiz, Q. Cui, A. G. Baboul, S. Clifford, J. Cioslowski, B. B. Stefanov, G. Liu, A. Liashenko, P. Piskorz, I. Komaromi, R. L. Martin, D. J. Fox, T. Keith, M. A. Al-Laham, C. Y. Peng, A. Nanayakkara, M. Challacombe, P. M. W. Gill, B. Johnson, W. Chen, M. W. Wong, C. Gonzalez and J. A. Pople, *GAUSSIAN 03 (Revision B.05)*, Gaussian Inc., Pittsburgh, PA, 2003.
33 R. Krishnan, M. J. Frisch and J. A. Pople, *J. Chem. Phys.*, 1980, **72**, 4244.
34 T. Clark, J. Chandrasekhar, G. W. Spitznagel and P. v. R. Schleyer, *J. Comput. Chem.*, 1983, **4**, 294.
35 C. Peng, P. Y. Ayala, H. B. Schlegel and M. J. Frisch, *J. Comput. Chem.*, 1996, **17**, 49.